Research Article

Paolo Franceschini, Andrea Tognazzi*, Anna M. Chernyak, Alexander I. Musorin, Alfonso C. Cino, Andrey A. Fedyanin and Costantino De Angelis

Enhancing second harmonic generation by Q-boosting lossless cavities beyond the time bandwidth limit

https://doi.org/10.1515/nanoph-2023-0389
Received June 27, 2023; accepted November 30, 2023;
published online January 2, 2024

Abstract: Nanostructures proved to be versatile platforms to control the electromagnetic field at subwavelength scale. Indeed, high-quality-factors nanocavities have been used to boost and control nonlinear frequency generation by increasing the light–matter interaction. However, nonlinear processes are triggered by high-intensities, which are provided by ultrashort laser pulses with large bandwidth, which cannot be fully exploited in such devices. Time-varying optical systems allow one to overcome the time-bandwidth limit by modulating the cavity external coupling. Here we present a general treatment, based on coupled mode theory, to describe second harmonic generation in a doubly resonant cavity for which the quality-factor at the fundamental frequency is modulated in time. We identify the initial quality factor maximizing second harmonic efficiency when performing Q-boosting and we predict a theoretical energy conversion efficiency close to unity. Our results have direct impact on the design of next generation time-dependent metasurfaces to boost nonlinear frequency conversion of ultrashort laser pulses.

Keywords: time-bandwidth limit; second harmonic generation; time-varying metasurface; Q-boosting

1 Introduction

Nonlinear optics has a variety of applications ranging from medicine to communication and laser frequency conversion [1–3]. The pump electric field intensity is one of the key factors determining nonlinear processes efficiency; thus, ultrashort laser pulses are often used, since they feature high peak intensities. Dielectric nanostructures represent a compact and versatile solution to control the phase, polarization, intensity, and electric field distribution on a subwavelength scale, broadening the functionalities offered by bulky crystals and down-scaling the device dimensions [4–10]. However, resonant structures are subject to the so-called time-bandwidth limitation, *i.e.*, the acceptance bandwidth of the device is $\approx\omega/Q$, where ω is the resonant radial frequency and Q is the quality-factor (Q-factor) [11]. Indeed, single resonators with low Q-factors ($Q < 50$) have short light–matter interaction time, which results in limited nonlinear conversion efficiency. On the other hand, metasurfaces and photonic crystals have larger Q-factors ($Q > 200$), which correspond to longer in-cavity lifetimes, but does not allow to couple all the incoming laser pulse spectrum to the device, ultimately limiting the performances. Overcoming the time-bandwidth limit is of paramount importance to fully exploit high-Q photonic devices, not only for nonlinear frequency conversion but also with any broadband radiation source. Previously, excitation with complex frequencies has been proposed to enhance coupling between the incoming radiation and the cavity [12, 13]. However, it is hard to sustain an exponentially increasing

***Corresponding author: Andrea Tognazzi**, National Institute of Optics – National Research Council (INO-CNR), Via Branze 45, 25123, Brescia, Italy; and Department of Engineering, University of Palermo, Viale delle Scienze ed. 9, 90128, Palermo, Italy, E-mail: andrea.tognazzi@unipa.it. https://orcid.org/0000-0002-5711-3917

Paolo Franceschini and Costantino De Angelis, Department of Information Engineering, University of Brescia, Via Branze 38, 25123, Brescia, Italy; and National Institute of Optics – National Research Council (INO-CNR), Via Branze 45, 25123, Brescia, Italy. https://orcid.org/0000-0001-5405-7668 (P. Franceschini). https://orcid.org/0000-0001-8029-179X (C. De Angelis)

Anna M. Chernyak, Alexander I. Musorin and Andrey A. Fedyanin, Faculty of Physics, Lomonosov Moscow State University, Leninskie gory 1, 119991, Moscow, Russia. https://orcid.org/0000-0001-9548-0008 (A. I. Musorin). https://orcid.org/0000-0003-4708-6895 (A. A. Fedyanin)

Alfonso C. Cino, Department of Engineering, University of Palermo, Viale delle Scienze ed. 9, 90128, Palermo, Italy

field amplitude profile over long time periods. In this framework, the possibility to tune the optical properties of metasurfaces with unprecedented speed, as fast as hundreds of fs [14–20], paved the way to devices operating beyond such limitation.

Time-variant metasurfaces allow to overcome the time-bandwidth tradeoff and extend metasurfaces functionalities [21–23]. Indeed recently, pulse generation and compression [24], coupling beyond the time bandwidth limit [25–28], spectral bandwidth manipulation [29–33], enhanced frequency conversion [34, 35] and light-storage [36, 37] were demonstrated. Coupled mode theory (CMT) represents a widespread tool to describe time-varying resonators [28, 38] and nonlinearities [39], since it can be applied from radio to optical frequencies. Although, CMT has been successfully applied to describe third harmonic generation at optical frequencies with time dependent Q-factors at the fundamental frequency (FF) [35], second harmonic generation (SHG) and the coupling between the fundamental and higher harmonic mode have yet to be considered. The underlying idea of this work, to efficiently transfer energy from FF to SH mode, is to couple the incoming laser pulse to a low-Q cavity and to modulate its Q-factor to increase the energy stored inside the resonator. This leads to an increased second harmonic (SH) conversion efficiency.

Here, we focus on doubly resonant cavities featuring an internal coupling between the modes at the fundamental and at its SH frequency. We provide a general treatment based on CMT (including also pump-depletion effects) to boost SHG of light pulses by modulating the external cavity coupling term at FF in a lossless doubly resonant cavity excited by an input pulse at FF. First, we extend the CMT model for SHG in Ref. [40] to a time-dependent doubly resonant cavity. Then, we study the role of time delay τ, *i.e.*, the time interval between the external pulse arrival and the instant at which the switching occurs. After that, we investigate the effect of the amplitude modulation of the Q-factor at the FF (before and after the switching) and compare our results with the static case, *i.e.*, when Q-factor is constant over time. We identify the initial and final Q-factor at the FF, and their relation with the external pulse duration, which maximize SH conversion. We demonstrate that the initial Q-factor plays a major role in boosting SHG. Our results pave the way to a deeper understanding of metasurfaces operating beyond the time bandwidth limit to boost nonlinear frequency conversion exploiting Q-boosting.

2 Results

2.1 Coupled mode theory for doubly-resonant second harmonic cavities

Here, we employ CMT to describe SHG in a doubly-resonant cavity, which supports modes at both FF, ω_1, and SH frequency, $\omega_2 = 2\omega_1$, with amplitudes a_1 and a_2, respectively [41]. The cavity is excited by an external source s_1^+, at frequency $\omega_p = \omega_1$ (resonant excitation). In general, the set of equations describing SHG in a doubly-resonant cavity is [40, 42]:

$$\begin{cases} \dfrac{\mathrm{d}a_1}{\mathrm{d}t} = \omega_1\left(i - \dfrac{1}{2Q_1}\right)a_1 - i\omega_1\,\beta_1 a_1^* a_2 + \sqrt{\dfrac{\omega_1}{Q_1}}\,s_1^+ \\ \dfrac{\mathrm{d}a_2}{\mathrm{d}t} = \omega_2\left(i - \dfrac{1}{2Q_2}\right)a_2 - i\omega_2\beta_2 a_1^2 \\ s_1^- = -s_1^+ + \sqrt{\dfrac{\omega_1}{Q_1}}\,a_1 \\ s_2^- = \sqrt{\dfrac{\omega_2}{Q_2}}\,a_2 \end{cases}, \quad (1)$$

where Q_1 and Q_2 are the Q-factors of modes 1 (FF) and 2 (SH), β_1 and β_2 are the internal cavity coupling coefficients, which are responsible for pump depletion and SH conversion, respectively, and they are related to the overlap integral between the FF and SH modes [40, 43]. As pointed out in Ref. [40], we set $\beta_2 = \beta_1/2$ to fulfill the conservation energy constraint. The terms s_1^- and s_2^- represent the outgoing waves at ω_1 and ω_2, respectively. Although not being explicitly reported, time dependence of a_k and $s_k^\pm$ terms in Equation (1) is implied. In analogy with [40], we define the SH (FF) power conversion efficiency as $\zeta_{SH} = P_2^-/P_1^+$ $\left(\zeta_{FF} = P_1^-/P_1^+\right)$, where P_2^- $\left(P_1^-\right)$ is the output power at ω_2 (ω_1) and P_1^+ is the input power at $\omega_p = \omega_1$. First, we focus on the SH power conversion within a cavity where Q_1 is constant over time (see Figure 1a). When the input source is a monochromatic continuous-plane-wave (CW), complete power conversion efficiency ($\zeta_{SH} = \left|s_{2,ss}^-\right|^2/\left|s_1^+\right|^2 = 1$ [40]) can be achieved for an optimum value of Q_1 $\left(Q_1^{\text{opt}}\right)$ in the steady state (ss) condition [40]. As an example, we calculate ζ_{SH} for various values of Q_1 by solving Equation (1) and we display the results as a function of the normalized

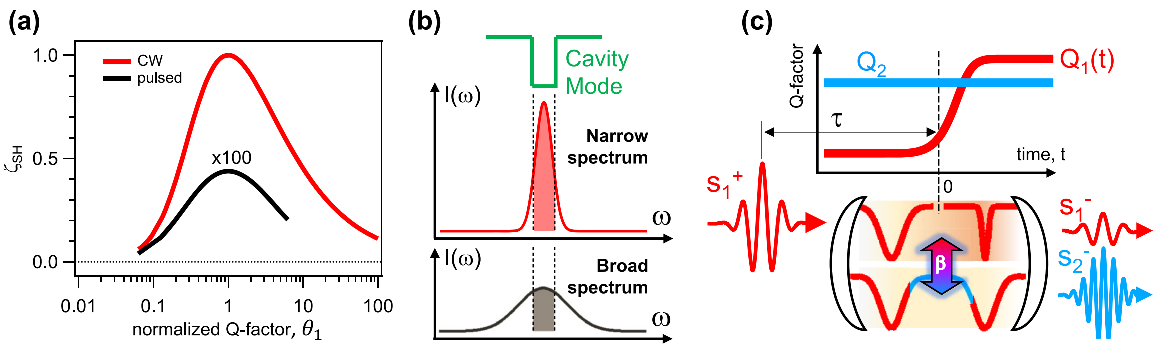

Figure 1: Framework and design of Q-boosting approach. (a) Static case second harmonic power conversion efficiency (ζ_{SH}) as a function of the normalized Q-factor ($\theta_1 = Q_1/Q_1^{\text{opt}}$) for a continuous-wave (CW, red curve) and pulsed (black curve, factor $\times$ 100 magnification) input sources s_1^+. For both CW and pulsed excitation cases, an optimal set of the cavity parameters exists (see Section 1 of the Supplementary Material). For both cases, quality factor of mode 2 (Q_2) is 1500. The value of internal coupling (β_1) is 1.5×10^{-4} $\sqrt{1/\text{J}}$ for the CW case and 1.5×10^{-4} $\sqrt{\text{fs/J}}$ for the pulsed case. (b) Amount of spectral power (shaded region) efficiently stored in a cavity mode (green line) for a narrow (red, top panel) and broadband pulse (black, bottom panel). (c) Time-dependent amplitude modulation (Equation (3)) of the Q-factor at ω_1 (Q_1) to enhance second harmonic conversion efficiency. The s_1^+ pulse resonantly excites the cavity mode at ω_1 (bottom panel). Given the coupling (β) between the cavity modes, by carefully tuning the temporal delay (τ) between the arrival of the pulse s_1^+ and the time at which the Q_1 modulation occurs, the relative amplitude of the outgoing waves at ω_1 (s_1^-) and $\omega_2 = 2\omega_1$ (s_2^-) can be controlled.

Q-factor $\left(\theta_1 = Q_1/Q_1^{\text{opt}}\right)$ in Figure 1a (red curve) for the following set of parameters: $\omega_1 = 0.791$ rad/fs ($\nu =$ 125.9 THz), $\beta_1 = 1.5 \times 10^{-4}$ $\sqrt{1/\text{J}}$, $Q_2 = 1500$, and $\left|s_1^+\right| = 17.33$ $\sqrt{\text{W}}$. The value of Q_1^{opt} is bounded to ω_1, β_1, Q_2 and $|s_1^+|^2$ [40] (see Section 1.1 of the Supplementary Material for more details).

Now, we consider a pulsed input source at resonance ($\omega_p = \omega_1$) with Gaussian temporal profile of the form:

$$s_1^+(t) = s_0 \cdot \sqrt[4]{(4\ \ln\ 2)/\left(\pi\tau_p^2\right)} \cdot \mathrm{e}^{-\frac{2\ \ln\ 2\ t^2}{\tau_p^2}} \cdot \mathrm{e}^{\mathrm{i}\omega_p t}, \tag{2}$$

where τ_p is the full width at half maximum (FWHM) of the time-dependent intensity profile $I(t) \propto \left|s_1^+(t)\right|^2$ and s_0 is the amplitude. $s_1^+(t)$ and $s_k^-(t)$ are the time-dependent amplitudes of the input and output waves, respectively [41]. In analogy with [34, 35], the quantity $U_k = \int_{-\infty}^{+\infty} \left|a_k(t)\right|^2 \mathrm{d}t$ defines the time-integrated energy (units [J s]) inside the cavity ascribed to the mode k and the pulse energy of the incoming and outgoing radiation (units [J]) are defined as $V_1^+ = \int_{-\infty}^{+\infty} \left|s_1^+(t)\right|^2 \mathrm{d}t = s_0^2$ and $V_k^- = \int_{-\infty}^{+\infty} \left|s_k^-(t)\right|^2 \mathrm{d}t$, respectively. Consequently, the input and output pulse power is calculated as the ratio between the pulse energy and its temporal duration: $P_k^\pm = V_k^\pm/\Delta t_k^\pm$ (see Supplementary Material for more details). For a pulsed source, the maximum achievable ζ_{SH} ($\zeta_{SH}^{\max}$) is much smaller than in the CW case. As shown by the black curve in Figure 1a, for $\tau_p = 100$ fs, $\beta_1 = 1.5 \times 10^{-4}$ $\sqrt{\text{fs/J}}$ and $s_0 = 17.33$ $\sqrt{\text{J}}$, $\zeta_{SH}^{\max} \simeq 0.44\,\%$ (see Supplementary Material). The difference with the monochromatic CW can be rationalized by recalling that, for a pulsed excitation, the spectral intensity profile ($S(\omega)$) has a bandwidth $\Delta\omega_p$, which is related to the transform-limited pulse duration τ_p by the time-bandwidth product: $\tau_p \cdot \Delta\omega_p = 4\ln 2$. Therefore, only the fraction of $S(\omega)$ matching the bandwidth of the cavity mode (shaded region in Figure 1b) is involved in the SH conversion process. A Q-boosting approach allow to increase the energy stored inside the cavity by a dynamic control of the Q-factor.

2.2 Time dependent *Q*-factor modulation

In Figure 1c, we depict the working principle of Q-boosting to enhance SHG. We consider a time-dependent amplitude modulation of Q_1 (occurring at $t = 0$), which, in the following part of the work, takes the form

$$\frac{1}{Q_1(t)} = \frac{1}{Q_{1L}} + \frac{1}{2}\left(\frac{1}{Q_{1H}} - \frac{1}{Q_{1L}}\right)\left[1 + \mathrm{erf}\left(\frac{t}{\sigma}\right)\right], \tag{3}$$

where σ is the switching time, Q_{1L} and Q_{1H} being the initial and final values of the FF Q-factor, respectively. In our model, the variation of Q corresponds to the change in the mode bandwidth γ, *i.e.*, $Q_1(t) = \omega_1/(2\gamma_1(t))$. Moreover, as sketched in Figure 1c, we allow the input pulse s_1^+ to enter the cavity with a delay time τ with respect to the instant at which Q_1 increases. Therefore, from Equation (2), the expression for s_1^+ becomes $s_1^+(t; \tau) = s_1^+(t - \tau)$. Here, the value of Q_2 is constant over time and, in the following, we assume $Q_2 = 1500$. In general, β_1 should change as the electric field distribution inside the cavity varies. Here, we assume those modifications to be negligible and consider β_1 to be constant over time.

First, we numerically solve Equation (1), endowed by the time-dependent Q_1 as in Equation (3) and assuming

$Q_{1L} = 55$ and $\sigma = 50$ fs. We introduce the modulation amplitude as $\rho = Q_{1H}/Q_{1L}$. The numerical results obtained for $\rho = 20$ are displayed in Figure 2a, which shows the temporal dynamics of the modes amplitude $|a_1(t)|^2$ and $|a_2(t)|^2$ (red and blue curve, respectively), excited by an input pulse with duration $\tau_p = 100$ fs and entering the cavity at $\tau = -40$ fs. The value of $|a_k(t)|^2$ $(k = 1, 2)$ is related to the instantaneous energy accumulated in the mode k [41] and decreases exponentially over time due to the $\omega_k/(2Q_k)a_k$ term in Equation (1). Here, we introduce the SH energy conversion efficiency as $\eta_{SH} = V_2^-/V_1^+$. At this stage it is important to underline that η_{SH} is related to ζ_{SH} through the term $\tau_p/\Delta t_2^-$ and the two frameworks allow to extract the same information (see Section 3 of the Supplementary Material). Therefore, we prefer to present the results in terms of η_{SH}. As displayed in the inset in Figure 2a, the optimum delay time (τ_{opt}), which maximizes the SH conversion efficiency, is $\tau_{\text{opt}} \approx -40$ fs (blue circle) and it is of the order of the resonator lifetime $Q_{1L}/\omega_1 \approx 70$ fs, consistent with [35]. Moreover, the inset in Figure 2a shows that, for $\tau \ll -\tau_p$, *i.e.*, the cavity has not switched yet, η_{SH} is the same as in the static case (SC, $\eta_{SH} \sim 7\,\%$) when $Q_1 = Q_{1L}$ (dashed purple line in Figure 2a, inset). On the other hand, for $\tau \gg \tau_p$, the input pulse enters the cavity when the switching has already occurred, thus the pulse essentially couples to a high-Q cavity, resulting in low η_{SH} (since a large portion of the incoming spectrum falls outside the cavity acceptance bandwidth). When $-\tau_p \lesssim \tau \lesssim \tau_p$, a large η_{SH} enhancement is achieved, since the radiation channel at the fundamental frequency reduces after a large portion of the incoming energy pulse has coupled to the cavity. In Figure 2a, η_{SH} increases from ~7 % to ~67 %. As expected, $\eta_{FF} = V_1^-/V_1^+$ decreases when η_{SH} increases.

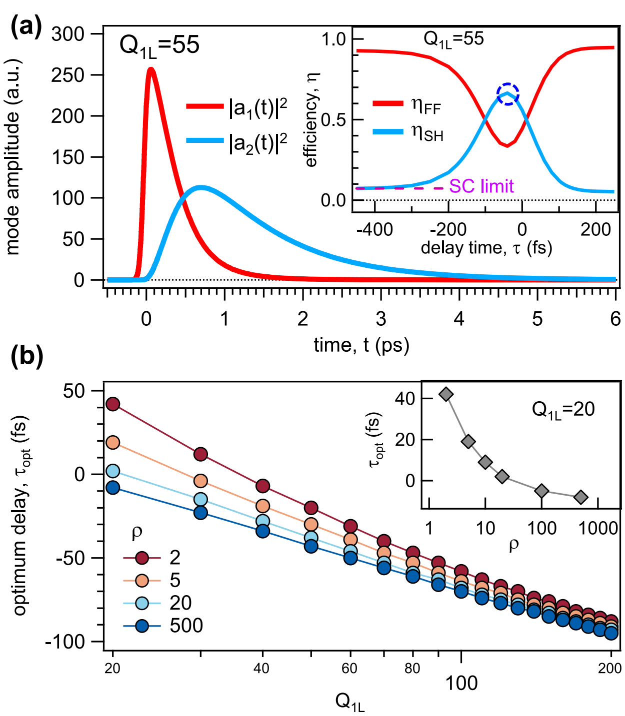

Figure 2: Coupled mode theory results within Q-boosted doubly resonant cavities. (a) Squared modulus of the fundamental frequency (FF) mode $|a_1|^2$ (red curve) and squared modulus of the second harmonic (SH) mode $|a_2|^2$ (blue curve) as a function of time t for $\tau = -40$ fs. The inset reports the FF (red curve) and SH (blue curve) conversion efficiency (η_{FF} and η_{SH}, respectively) as a function of the temporal delay τ. The blue circle highlights the optimum delay $\tau^{\text{opt}} \approx -40$ fs case. SC: static case. (b) τ^{opt} as a function of the initial quality-factor Q_{1L} for different ratios $\rho = Q_{1H}/Q_{1L}$, where Q_{1H} is the final quality-factor. The inset reports τ^{opt} as a function of ρ for $Q_{1L} = 20$.

Now, we discuss how τ_{opt} relates to ρ. In Figure 2b, we report τ^{opt} as a function of Q_{1L} for different Q-factor ratios $\rho = Q_{1H}/Q_{1L}$ with $\tau_p = 100$ fs (see Section 2 of the Supplementary Material for more details). For $\rho \lesssim 20$ and $Q_{1L} \lesssim 30$, τ^{opt} is positive, meaning that the switch should occur before the pulse enters the cavity. Moreover, for small Q_{1L}, τ^{opt} strongly depends on ρ, while for large Q_{1L}, τ^{opt} becomes almost independent from ρ (see the inset in Figure 2b). We note that as Q_{1L} increases, τ^{opt} becomes negative for all values of ρ, meaning that the switching should occur once the pulse is already inside the cavity. The inset in Figure 2b shows that, for a fixed Q_{1L}, τ is critical only for small values of ρ. This is of particular interest since, in practice, small ρ are easier to induce and different ways to dynamically manipulate a cavity Q-factor have already been proposed [15, 16, 35, 44]. However, we stress that our model can be applied to a wider class of doubly resonant cavities beyond metasurfaces. Therefore, the results shown in Figure 2b allow identifying the relevant timescale regarding the tuning of the delay time τ.

In the following, we focus only on the dependence of SH conversion efficiency upon Q_{1L} and Q_{1H}, since a more detailed analysis of the exact dependence of τ^{opt} on the other relevant parameters is beyond the scope of the present work. We calculate the optimum values of Q_{1L} and Q_{1H}, denoted as Q_{1L}^{opt} and Q_{1H}^{opt}, which maximize η_{SH}, by computing:

$$\max_{\tau} \eta_{SH}(Q_{1L}, Q_{1H}, \tau).$$

In Figure 3a, we report η_{SH} as a function of Q_{1L} for different ρ values. The black curve corresponds to the static case ($Q_1 = Q_{1L} = Q_{1H} \to \rho = 1$) and the purple triangle highlights the maximum SH conversion efficiency (η_{SH}^{max}) for the static case. We note that, at constant Q_{1L}, η_{SH} increases with increasing ρ. Indeed, an increasing Q_{1H} value corresponds to a decrease of the radiative losses of the FF mode; thus, the energy transferred from the FF to the SH mode (through the internal coupling term β_2) increases. The vertical arrow

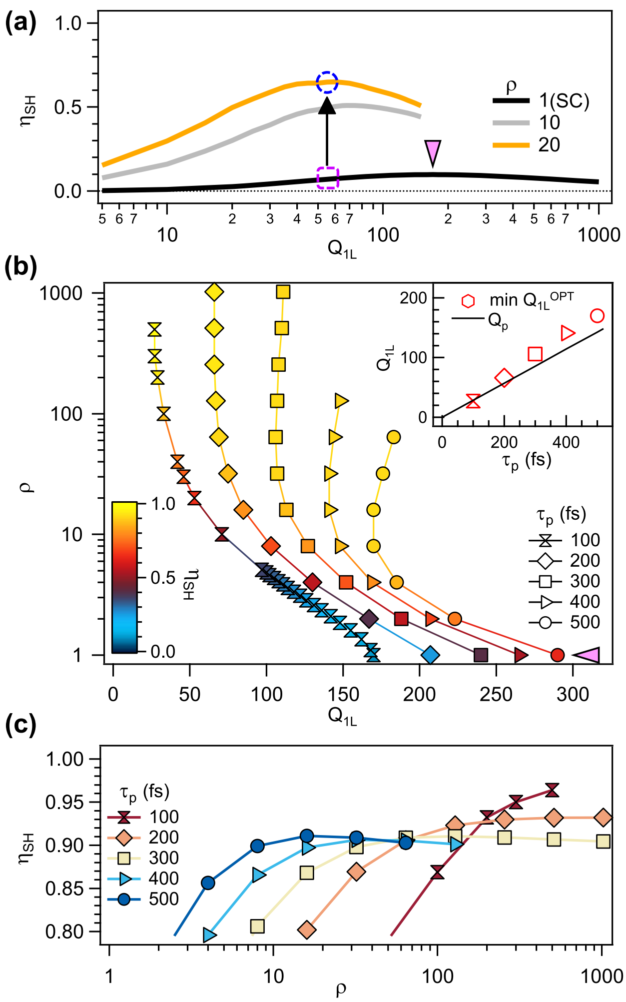

Figure 3: Optimal configurations for efficiency enhancement. (a) Second harmonic conversion efficiency (η_{SH}) at the optimum delay time (τ^{opt}) as a function of the initial quality-factor (Q_{1L}) for different values of $\rho = Q_{1H}/Q_{1L}$, where Q_{1H} is the final Q-factor: 1 (black curve, static case), 10 (gray curve), and 20 (yellow curve). The black vertical arrow highlights the η_{SH} enhancement for $Q_{1L} = 55$ (case displayed in Figure 2a). (b) Combinations of Q_{1L} and ρ at τ^{opt} leading to maximum η_{SH}, for different impinging pulse duration (τ_p). The value of η_{SH} is indicated by the colorscale. The inset reports the Q_{1L} corresponding to maximum η_{SH} as a function of τ_p. The black line corresponds to the bandwidth-matching condition $\omega_1/(Q_{1L}) = 1/\tau_p$. (c) η_{SH} as a function of ρ for different τ_p. For each ρ^{opt}, it is possible to extract the corresponding Q_{1L}^{opt} from panel (b). In the panels, the pink triangles indicates the maximum conversion efficiency in the static case ($\rho = 1$).

highlights what happens in a Q-boosted cavity, *i.e.*, fixed τ_p and ω_1, for $Q_{1L} = 55$ (reference case in Figure 2a). A suitable choice of Q_{1L} and Q_{1H} values allows to enhance η_{SH} (blue circle) compared to the static case (violet square). The maximum conversion efficiency is attained for a Q_{1L} which is different from the optimal Q_1 in the static case. We also note that Q_{1L}^{opt} decreases as ρ increases.

In order to formulate useful guidelines for time-dependent doubly resonant cavities operation, we report in Figure 3b the trajectories (for various τ_p values), in the plane spanned by Q_{1L} and ρ, allowing a SH efficiency enhancement. Within a curve, each point represents the value of Q_{1L} which maximizes η_{SH} (*i.e.*, Q_{1L}^{opt}) at a given ρ and the colorscale highlights the corresponding SH efficiency value. At fixed τ_p, Q_{1L}^{opt} gradually shifts from the initial static case ($\rho = 1$, purple triangle) toward lower values and reaches, for increasing ρ, a minimum value Q_{1L}^{min}, which corresponds to η_{SH}^{max} (see Figure 3c). From Figure 3b inset, we note that $Q_{1L}^{\mathrm{min}} \sim Q_p = \omega_p \tau_p/(4 \ln 2)$, where Q_p is an effective Q-factor given by the parameters describing the control pulse; therefore, Q_{1L}^{min} is close, but not equal, to the bandwidth-matching condition.

In order to qualitatively explain the relation between Q_{1L}^{min} and Q_p, we have to briefly discuss the properties of the spectral profile of the entities involved (see Section 3 of the Supplementary Material for more details). In the frequency domain, the spectral lineshape of the excited-wave amplitude within a resonant lossy system (at FF mode) is given by a Lorentzian function [25]

$$\mathcal{L}_{FF}(\omega; \Gamma) = \frac{1}{\pi} \cdot \frac{(\Gamma/2)^2}{(\Gamma/2)^2 + (\omega - \omega_1)^2}, \tag{4}$$

where Γ represents the spectral linewidth (FWHM). On the other hand, given the choice of the temporal profile of the control pulse in Equation (2), its spectral shape is given by a Gaussian function:

$$\mathcal{G}(\omega) = \sqrt{\frac{4 \ln 2}{\pi\, \Delta\omega_p^2}}\, \exp\left[-\frac{4 \ln 2}{\Delta\omega_p^2} \cdot (\omega - \omega_1)^2\right]. \tag{5}$$

The SH conversion process involves an effective energy transfer from the input pulse (s_1^+) to the FF mode via the external coupling coefficient and then a transfer to the SH mode through the internal coupling term β. To do so efficiently, it is required to suitably match the spectral energy, within a certain spectral interval (delimited by ω_A and ω_B), of the input pulse and the FF mode. The optimal matching condition between $\mathcal{L}_{FF}$ and $\mathcal{G}$, centered at ω_1, is given by:

$$\int_{\omega_A}^{\omega_B} \mathrm{d}\omega\, \mathcal{G}(\omega) = \int_{\omega_A}^{\omega_B} \mathrm{d}\omega\, \mathcal{L}_{FF}(\omega; \tilde{\Gamma}) \tag{6}$$

with $\omega_{A,B} = \omega_1 \mp \Delta\omega_p$, which leads to $\tilde{\Gamma}/\Delta\omega_p \simeq 0.4 < 1$ (see Section 3 of the Supplementary Material). Thus, the matched cavity bandwidth $\tilde{\Gamma}$ satisfies the relation: $\tilde{\Gamma} < \Delta\omega_p$.

From Figure 3b, we note that the ρ value at which Q_{1L}^{min} occurs decreases with increasing τ_p, suggesting that, for long τ_p values, $\rho \simeq 1$. This is consistent with the results obtained for the monochromatic CW case [40] (corresponding to $\tau_p \to \infty$), for which a complete SH conversion efficiency is observed in the steady state regime of constant Q-factor ($\rho = 1$).

As noted in Figure 3c, η_{SH} decreases for $\rho > \rho^{\text{opt}}$. This means that, after reaching ρ^{opt}, a further increase of the cavity acceptance bandwidth is of little use, since the spectral weight of the frequencies far from ω_1 is negligible. Ideally, despite the pump depletion term (β_1) is included, for an infinite value of Q_{1H} and very long time, all the radiation stored in a_1 can only escape through mode a_2. This is because increasing Q_{1H} corresponds to closing the only radiation channel of mode a_1, thus the energy can only escape the cavity through frequency conversion to ω_2, since the radiation channel of mode a_2 remains open. As expected from energy conservation $\eta_{SH} < 1$ and significantly increases for shorter pulses. It is clear that ρ^{opt} decreases as τ_p becomes longer.

2.3 Limitations and implementation strategies

The modulation of the external coupling parameter Q_1 may have consequences from a spectral point of view, thus potentially limiting the validity of the model. Indeed, an abrupt amplitude modulation of the Q-factor might: (*i*) introduce additional components in the spectrum of a_1 (a_2) located far from the central frequency ω_1 (ω_2) in the neighborhood of ω_2 (ω_1) or (*ii*) induce a significant frequency shift of the modes. Regarding the former aspect, the most delicate point is related to the switching time parameter σ, *i.e.*, the speed at which the variation of Q_1 occurs, compared to the optical cycle of the input pulse $2\pi/\omega_1$. In our work, $\sigma = 50$ fs and $\tau_p = 100$ fs. This means that, given the Q-factor dynamics in Equation (3), the time interval required to go from 10 % to 90 % of the entire variation is ~70 fs, which is nearly 10 times larger than $2\pi/\omega_1 \sim 7.9$ fs. Therefore, although σ and τ_p are comparable, in the time interval $2\pi/\omega_1$, the pulse intensity and the Q-factor can be assumed as constant. Regarding the latter aspect, to limit the impact of frequency shift in Q-boosting, specific conditions in refractive index and loss changes can be adopted in practical realizations [32], as demonstrated by FDTD simulations in Ref. [35]. The validity of our approach is further confirmed by continuous wavelet analysis of the modes dynamics [27], which reveal that the modes have a constant central frequency (see Section S5 of Supplementary Material).

For the effective implementation of this scheme in the case of broadband pulses, a large variation between the initial and final values of the cavity Q-factor is required to obtain a high SH conversion efficiency, as previously discussed. The practical realization of this can be achieved by the suitable design of a cavity endowed by a material-dependent sharp resonance, *e.g.*, a quasi-BIC, at fundamental frequency. Thanks to a control light pulse, a variation of the material dielectric function [45, 46] can be induced, which in turn causes a large modulation of the Q-factor amplitude at FF with small frequency shift. A model including large frequency shift of the fundamental and/or SH modes is beyond the scope of this work. In order to avoid two-photon absorption and free carrier generation effects, an external control pulse with energy smaller than half of the bandgap may be used as in $LiNbO_3$ and other large bandgap materials with non-zero $\chi^{(2)}$ [47]. Further theoretical development may take into account the role of non-radiative losses which may arise from free-carrier excitation or two-photon absorption. Other suitable platforms include dielectric slabs featuring a BIC mode which can be coupled to external radiation by means of a transient grating [48]. In such platforms the Q-factor can be dramatically increased in a short time by removing the transient grating, thus reducing any possible non-radiative loss and at the same time achieving a long-lived high-Q resonant condition.

3 Conclusions

To conclude, we have unveiled how to maximize SH efficiency in a Q-boosted doubly resonant cavity. First, by applying CMT, we have compared SHG for static and modulated Q-factors, and predicted that η_{SH} can be significantly increased in time-dependent cavities. Secondly, we have shown that the first parameter to be optimized should be the delay time, which must be carefully chosen depending on the initial and final Q-factors. In particular, the optimum delay goes from positive to negative values when Q_{1H}/Q_{1L} increases. For proper delay time and Q_{1H}/Q_{1L}, we have predicted SH efficiency conversion close to unity.

We have shown that perfect bandwidth-matching between cavity and pulse cannot be achieved due to different lineshapes. Thus, Q_{1L}^{opt} is the one maximizing the overlap between a Gaussian and a Lorentizan. Additionally, we have found that the maximum conversion efficiency is not achieved when the cavity radiative losses at the fundamental becomes zero, *i.e.*, $Q_{1H} \to +\infty$. Instead, its value is determined by a compromise between a lower value, allowing a full collection of photons inside the cavity, and a longer cavity lifetime. Moreover, as the pulse duration increases, Q_{1H}^{opt} and Q_{1L}^{opt} get closer values; ultimately leading to the CW static case when $\tau_p \to +\infty$.

Here, we have shown that both low-Q and high-Q resonators benefit from this approach. The formulated guidelines to efficiently perform Q-boosting of nanoresonators and metasurfaces pave the way to achieve large conversion efficiency in finite-size nanophotonic system by dynamically increasing the Q-factor.

Acknowledgment: The authors acknowledge stimulating discussions with Tal Ellenbogen. A. Tognazzi acknowledges the financial support from the European Union through "FESR o FSE, PON Ricerca e Innovazione 2014–2020 – DM 1062/2021" and the University of Palermo through "Fondo Finalizzato alla Ricerca di Ateneo 2023 (FFR2023)".

Research funding: The authors acknowledge the financial support from the European community through the "METAFAST" project (H2020-FETOPEN-2018-2020, grant agreement no. 899673), and Ministero Italiano dell'Istruzione (MIUR) through the "METEOR" project (PRIN-2020, 2020EY2LJT_002).

Author contributions: All authors have accepted responsibility for the entire content of this manuscript and approved its submission.

Conflict of interest: Authors state no conflict of interest.

Data availability: All data generated or analyzed during this study are included in this published article and its supplementary information files.

References

[1] E. Garmire, "Nonlinear optics in daily life," *Opt. Express*, vol. 21, no. 25, p. 30532, 2013.

[2] T. Schneider, *Nonlinear Optics in Telecommunications. Advanced Texts in Physics*, London, Springer London, Limited, 2013.

[3] Y. Zhao, Y. Yang, and H.-B. Sun, "Nonlinear meta-optics towards applications," *PhotoniX*, vol. 2, no. 1, p. 3, 2021.

[4] M. Kauranen and A. V. Zayats, "Nonlinear plasmonics," *Nat. Photonics*, vol. 6, no. 11, pp. 737–748, 2012.

[5] A. F. Koenderink, A. Alù, and A. Polman, "Nanophotonics: shrinking light-based technology," *Science*, vol. 348, no. 6234, pp. 516–521, 2015.

[6] A. I. Kuznetsov, A. E. Miroshnichenko, M. L. Brongersma, Y. S. Kivshar, and B. Luk'yanchuk, "Optically resonant dielectric nanostructures," *Science*, vol. 354, no. 6314, p. 846, 2016.

[7] L. Carletti, K. Koshelev, C. De Angelis, and Y. Kivshar, "Giant nonlinear response at the nanoscale driven by bound states in the continuum," *Phys. Rev. Lett.*, vol. 121, no. 3, p. 033903, 2018.

[8] A. Krasnok, M. Tymchenko, and A. Alù, "Nonlinear metasurfaces: a paradigm shift in nonlinear optics," *Mater. Today*, vol. 21, no. 1, pp. 8–21, 2018.

[9] Y. Kivshar, "All-dielectric meta-optics and non-linear nanophotonics," *Natl. Sci. Rev.*, vol. 5, no. 2, pp. 144–158, 2018.

[10] A. Tognazzi, K. I. Okhlopkov, A. Zilli, et al., "Third-harmonic light polarization control in magnetically resonant silicon metasurfaces," *Opt. Express*, vol. 29, no. 8, p. 11605, 2021.

[11] D. A. B. Miller, "Fundamental limit to linear one-dimensional slow light structures," *Phys. Rev. Lett.*, vol. 99, no. 20, p. 203903, 2007.

[12] D. G. Baranov, A. Krasnok, and A. Alù, "Coherent virtual absorption based on complex zero excitation for ideal light capturing," *Optica*, vol. 4, no. 12, p. 1457, 2017.

[13] S. Kim, S. Lepeshov, A. Krasnok, and A. Alù, "Beyond bounds on light scattering with complex frequency excitations," *Phys. Rev. Lett.*, vol. 129, no. 20, p. 203601, 2022.

[14] M. R. Shcherbakov, P. P. Vabishchevich, A. S. Shorokhov, et al., "Ultrafast all-optical switching with magnetic resonances in nonlinear dielectric nanostructures," *Nano Lett.*, vol. 15, no. 10, pp. 6985–6990, 2015.

[15] G. D. Valle, B. Hopkins, L. Ganzer, et al., "Nonlinear anisotropic dielectric metasurfaces for ultrafast nanophotonics," *ACS Photonics*, vol. 4, no. 9, pp. 2129–2136, 2017.

[16] M. R. Shcherbakov, S. Liu, V. V. Zubyuk, et al., "Ultrafast all-optical tuning of direct-gap semiconductor metasurfaces," *Nat. Commun.*, vol. 8, no. 1, p. 17, 2017.

[17] L. Carletti, D. de Ceglia, M. A. Vincenti, and C. De Angelis, "Self-tuning of second-harmonic generation in GaAs nanowires enabled by nonlinear absorption," *Opt. Express*, vol. 27, no. 22, p. 32480, 2019.

[18] P. Franceschini, L. Carletti, A. P. Pushkarev, et al., "Tuning the ultrafast response of fano resonances in halide perovskite nanoparticles," *ACS Nano*, vol. 14, no. 10, pp. 13602–13610, 2020.

[19] L. Carletti, M. Gandolfi, D. Rocco, et al., "Reconfigurable nonlinear response of dielectric and semiconductor metasurfaces," *Nanophotonics*, vol. 10, no. 17, pp. 4209–4221, 2021.

[20] T. Ning, X. Li, Z. Zhang, et al., "Ultimate conversion efficiency of second harmonic generation in all-dielectric resonators of quasi-BICs in consideration of nonlinear refraction of dielectrics," *Opt. Express*, vol. 29, no. 11, p. 17286, 2021.

[21] Y. Tanaka, J. Upham, T. Nagashima, T. Sugiya, T. Asano, and S. Noda, "Dynamic control of the Q factor in a photonic crystal nanocavity," *Nat. Mater.*, vol. 6, no. 11, pp. 862–865, 2007.

[22] A. M. Shaltout, V. M. Shalaev, and M. L. Brongersma, "Spatiotemporal light control with active metasurfaces," *Science*, vol. 364, no. 6441, p. eaat3100, 2019.

[23] E. Galiffi, R. Tirole, S. Yin, et al., "Photonics of time-varying media," *Adv. Photon.*, vol. 4, no. 1, p. 014002, 2022.

[24] K. Kondo, N. Ishikura, T. Tamura, and T. Baba, "Temporal pulse compression by dynamic slow-light tuning in photonic-crystal waveguides," *Phys. Rev. A*, vol. 91, no. 2, p. 023831, 2015.

[25] K. L. Tsakmakidis, L. Shen, S. A. Schulz, et al., "Breaking Lorentz reciprocity to overcome the time-bandwidth limit in physics and engineering," *Science*, vol. 356, no. 6344, pp. 1260–1264, 2017.

[26] Z. Hayran and F. Monticone, "Capturing broadband light in a compact bound state in the continuum," *ACS Photonics*, vol. 8, no. 3, pp. 813–823, 2021.

[27] L. Cong, J. Han, W. Zhang, and R. Singh, "Temporal loss boundary engineered photonic cavity," *Nat. Commun.*, vol. 12, no. 1, p. 6940, 2021.

[28] D. L. Sounas, "Virtual perfect absorption through modulation of the radiative decay rate," *Phys. Rev. B*, vol. 101, no. 10, p. 104303, 2020.

[29] K. Lee, J. Son, J. Park, et al., “Linear frequency conversion via sudden merging of meta-atoms in time-variant metasurfaces,” *Nat. Photonics*, vol. 12, no. 12, pp. 765—773, 2018.
[30] E. Galiffi, P. A. Huidobro, and J. B. Pendry, “Broadband nonreciprocal amplification in luminal metamaterials,” *Phys. Rev. Lett.*, vol. 123, no. 20, p. 206101, 2019.
[31] Y. Zhou, M. Z. Alam, M. Karimi, et al., “Broadband frequency translation through time refraction in an epsilon-near-zero material,” *Nat. Commun.*, vol. 11, no. 1, p. 2180, 2020.
[32] V. V. Zubyuk, P. A. Shafirin, M. R. Shcherbakov, G. Shvets, and A. A. Fedyanin, “Externally driven nonlinear time-variant metasurfaces,” *ACS Photonics*, vol. 9, no. 2, pp. 493—502, 2022.
[33] R. Tirole, E. Galiffi, J. Dranczewski, et al., “Saturable time-varying mirror based on an epsilon-near-zero material,” *Phys. Rev. Appl.*, vol. 18, no. 5, p. 054067, 2022.
[34] M. R. Shcherbakov, P. Shafirin, and G. Shvets, “Overcoming the efficiency-bandwidth tradeoff for optical harmonics generation using nonlinear time-variant resonators,” *Phys. Rev. A*, vol. 100, no. 6, p. 063847, 2019.
[35] P. A. Shafirin, V. V. Zubyuk, A. A. Fedyanin, and M. R. Shcherbakov, “Nonlinear response of Q-boosting metasurfaces beyond the time-bandwidth limit,” *Nanophotonics*, vol. 11, no. 17, pp. 4053—4061, 2022.
[36] J. Upham, Y. Fujita, Y. Kawamoto, et al., “The capture, hold and forward release of an optical pulse from a dynamic photonic crystal nanocavity,” *Opt. Express*, vol. 21, no. 3, p. 3809, 2013.
[37] M. F. Yanik and S. Fan, “Stopping light all optically,” *Phys. Rev. Lett.*, vol. 92, no. 8, p. 083901, 2004.
[38] H. Li and A. Alù, “Temporal switching to extend the bandwidth of thin absorbers,” *Optica*, vol. 8, no. 1, p. 24, 2020.
[39] G. D. Aguanno, M. Centini, M. Scalora, et al., “Generalized coupled-mode theory for $\chi^{(2)}$ interactions in finite multilayered structures,” *J. Opt. Soc. Am. B*, vol. 19, no. 9, p. 2111, 2002.
[40] A. Rodriguez, M. Soljacic, J. D. Joannopoulos, and S. G. Johnson, “$\chi^{(2)}$ and $\chi^{(3)}$ harmonic generation at a critical power in inhomogeneous doubly resonant cavities,” *Opt. Express*, vol. 15, no. 12, p. 7303, 2007.
[41] H. A. Haus, *Waves and Fields in Optoelectronics*, Englewood Cliffs, New Jersey, Prentice-Hall, 1984, p. 402.
[42] Z. Lin, X. Liang, M. Lončar, S. G. Johnson, and A. W. Rodriguez, “Cavity-enhanced second-harmonic generation via nonlinear-overlap optimization,” *Optica*, vol. 3, no. 3, p. 233, 2016.
[43] S. Zanotti, M. Minkov, S. Fan, L. C. Andreani, and D. Gerace, “Doubly-resonant photonic crystal cavities for efficient second-harmonic generation in III—V semiconductors,” *Nanomaterials*, vol. 11, no. 3, p. 605, 2021.
[44] G. Sartorello, N. Olivier, J. Zhang, et al., “Ultrafast optical modulation of second- and third-harmonic generation from cut-disk-based metasurfaces,” *ACS Photonics*, vol. 3, no. 8, pp. 1517—1522, 2016.
[45] S. I. Azzam and A. V. Kildishev, “Photonic bound states in the continuum: from basics to applications,” *Adv. Opt. Mater.*, vol. 9, no. 1, p. 2001469, 2020.
[46] J. Upham, H. Inoue, Y. Tanaka, et al., “Pulse capture without carrier absorption in dynamic Q photonic crystal nanocavities,” *Opt. Express*, vol. 22, no. 13, p. 15459, 2014.
[47] I. A. Kulagin, R. A. Ganeev, R. I. Tugushev, A. I. Ryasnyansky, and T. Usmanov, “Components of the third-order nonlinear susceptibility tensors in KDP, DKDP and $LiNbO_3$ nonlinear optical crystals,” *Quantum Electron.*, vol. 34, no. 7, pp. 657—662, 2004.
[48] H. J. Eichler, P. Günter, and D. W. Pohl, *Laser-Induced Dynamic Gratings. Vol. 50. Springer Series in Optical Sciences*, Berlin, Springer Berlin Heidelberg, 1986.

Supplementary Material: This article contains supplementary material (https://doi.org/10.1515/nanoph-2023-0389).